



Rosa, L., Buividas, R., Juodkazis, S., Kondo, T. & Masuda, H. (2011). Alumina-embedded Au nanowires for SERS sensing.

Originally published in *Proceedings of the International Workshop on Biophotonics (BioPhotonics 2011), Parma, Italy, 08-10 June 2011*. Piscataway, NJ: IEEE.

Available from: <http://dx.doi.org/10.1109/IWBP.2011.5954854>

Copyright © 2011 IEEE.

This is the author's version of the work. It is posted here with the permission of the publisher for your personal use. No further distribution is permitted. If your library has a subscription to these conference proceedings, you may also be able to access the published version via the library catalogue.



# Alumina-Embedded Au Nanowires for SERS Sensing

Lorenzo Rosa, Ričardas Buividas, Saulius Juodkazis  
Applied Plasmonics, Centre for Micro-Photonics  
Swinburne University of Technology  
P.O.Box 218, Hawthorn, VIC 3122, Australia  
[lrosa@ieee.org](mailto:lrosa@ieee.org)

Toshiaki Kondo, Hideki Masuda  
Kanagawa Academy of Science and Technology  
Sagamihara, Kanagawa 22-1131, Japan

**Abstract**— We propose a novel substrate for SERS bio-sensing composed of an hexagonal array of gold nanorods embedded in an anodically-oxidized alumina substrate, reaching a surface field enhancement up to 220 times.

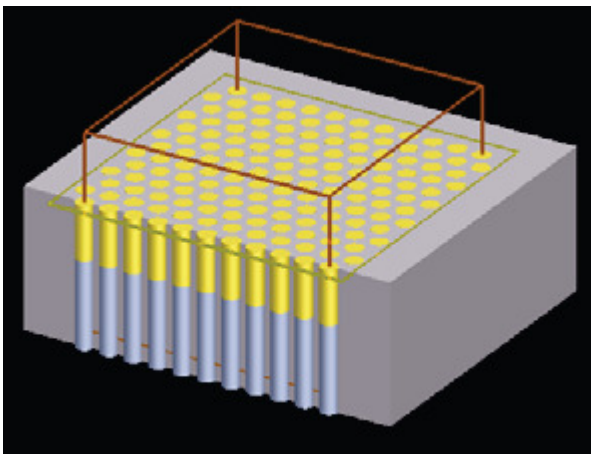


Figure 1. Simulation domain: nanorods of height  $h$  embedded in AAO.

## I. INTRODUCTION

Anodically-oxidized alumina (AAO) [1] is a unique nanostructured material which can be prepared over macroscopic large areas with superb quality and fidelity, high resolution of nanopores down to tens-of-nanometers, and high aspect ratio. Free standing films of AAO pores filled with electrochemically deposited gold have applications in bio-sensing and Raman scattering [2]. Plasmonic functionality of Au-filled pores makes the AAO membrane spectrally selective in scattering light. This applies to microscopic detection of weak luminescence in cell-biology microscopic applications. We model the optical properties of the AAO-Au membranes.

The structure is shown in Fig. 1, and is composed of a hexagonal array of gold nanowires of height  $h = 310$  nm and diameter of 70 nm, embedded in a AAO substrate. The center-to-center distance is 100 nm, the nanowire ends are flush with the upper surface, and air holes extend from their lower end for the whole thickness of the substrate.

## II. NUMERICAL SIMULATION

The structure performance was simulated by the 3D-FDTD method using the Lumerical software package. The simulation domain of  $1 \mu\text{m}^3$  volume is indicated by the brown box in Fig. 1, and the yellow square is the surface field enhancement monitor. The substrate thickness was set to  $1 \mu\text{m}$ , where the field values were considered negligible with respect to the surface. PML boundary conditions enclose the simulation on the top and bottom boundaries, and periodic boundary conditions are placed on the  $x$ - and  $y$ -boundaries. The array was illuminated by a linearly polarized total field-scattered field source alternatively  $x$ - and  $y$ -polarized, to detect cross-sections and maximum field enhancement. The materials losses were realistically simulated by introducing complex refractive index values tabulated in literature and available in the Lumerical materials library.

## III. RESULTS

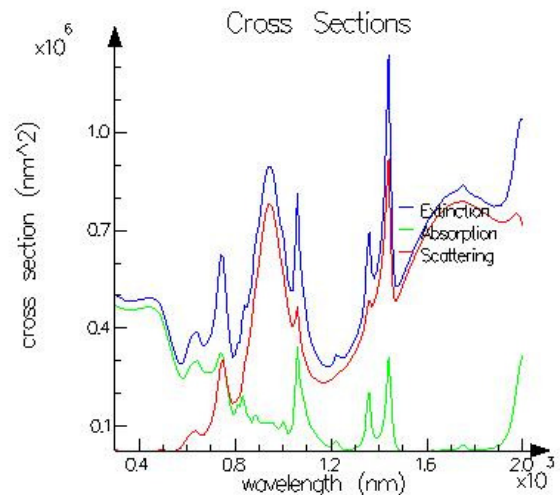


Figure 2. Extinction, absorption, and scattering cross-sections vs. wavelength.

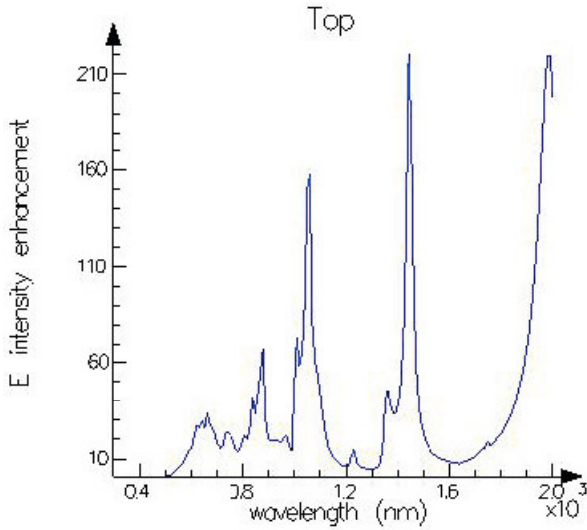


Figure 3. Surface E-field intensity enhancement vs. wavelength for  $x$  - polarized source.

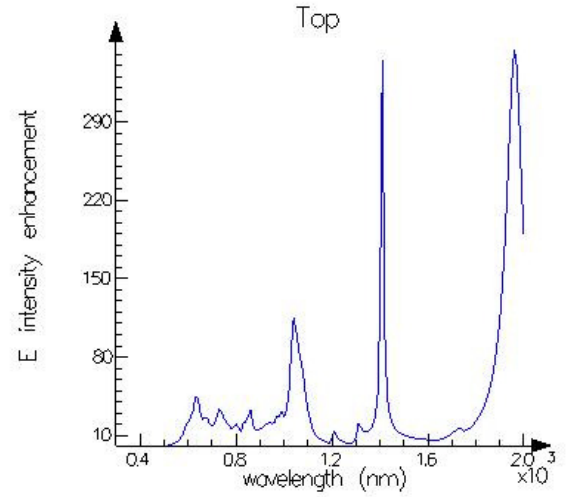


Figure 5. Surface E-field intensity enhancement vs. wavelength for  $y$  - polarized source.

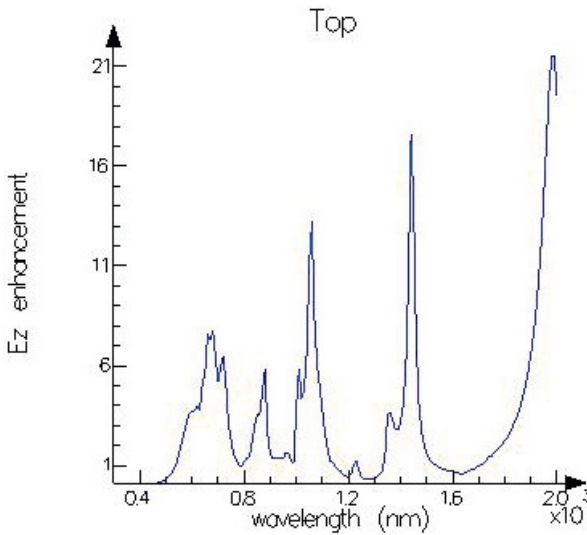


Figure 4. Surface  $E_z$  intensity enhancement vs. wavelength for  $x$  - polarized source.

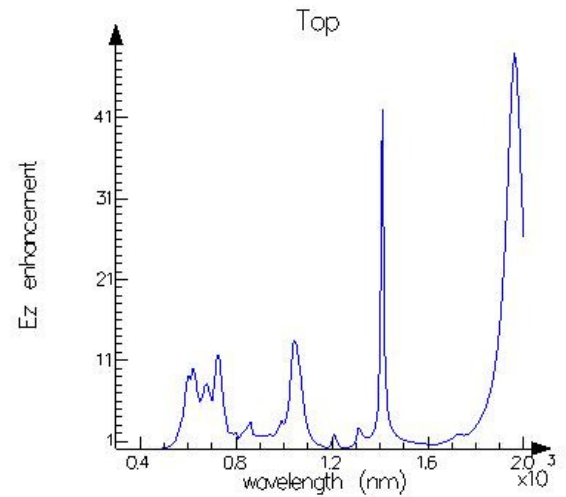


Figure 6. Surface  $E_z$  intensity enhancement vs. wavelength for  $y$  - polarized source.

The simulation was performed between 300 and 2000 nm wavelength, and the cross-section data, shown in Fig. 2, show only slight differences between  $x$ - and  $y$ -polarization. In both cases, they suggest a significant absorption up to 800 nm wavelength, while they present three main scattering peaks located at 950, 1440 (1410 for  $y$ -polarization), and 1750 nm. These are related to the plasmonic resonances which control field enhancement at the interface between the sensor and the measured substance.

In fact, as we show in Fig. 3 for  $x$ -polarization, we have three strong  $|E|^2$  enhancement peaks at 1070, 1440, and 1980 nm, with enhancement values of 160, 220, and 220, respectively. As the two outer peaks are off to the side of the respective scattering peaks, we consider them as dark plasmons. As shown in Fig. 4, about 10% enhancement (with

values of 13, 17, and 22, respectively) relates to the  $E_z$  component, important as it governs surface carrier extraction.

In Fig. 5 we show for  $y$ -polarization that the same  $|E|^2$  enhancement peaks are slightly moved to 1050, 1410, and 1950 nm, due to the slightly different effective distance between the rods along that axis, with enhancement values of 115, 340, and 350, respectively. The same reasoning as before applies to the two outer peaks, which we classify as dark plasmons. As shown in Fig. 6, the  $E_z$  component enhancement fraction is higher in this case, about 12% to 15%, with values of 14, 42, and 49, respectively.

In Figs. 7 to 10 we show the field configurations for the central peak, corresponding to the maximum extinction. In particular, in Fig. 7 we observe the field intensity enhancement on the substrate interface for  $x$ -polarization, focusing on the

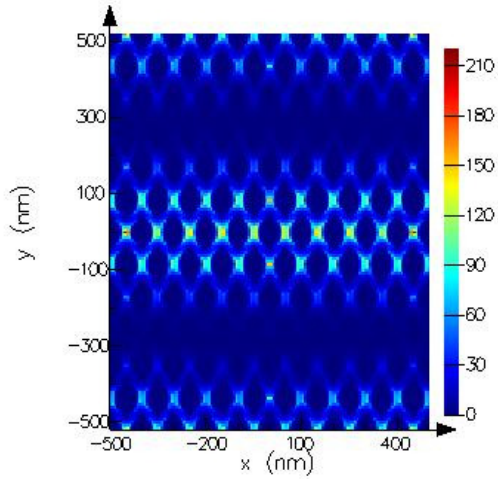


Figure 7. Surface intensity enhancement at 1440 nm for  $x$ -pol. source.

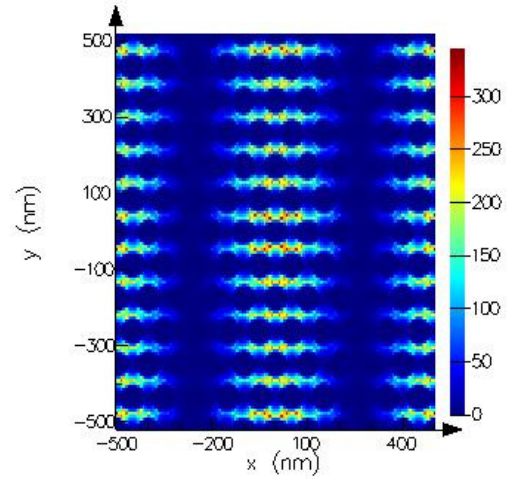


Figure 9. Surface intensity enhancement at 1410 nm for  $y$ -pol. source.

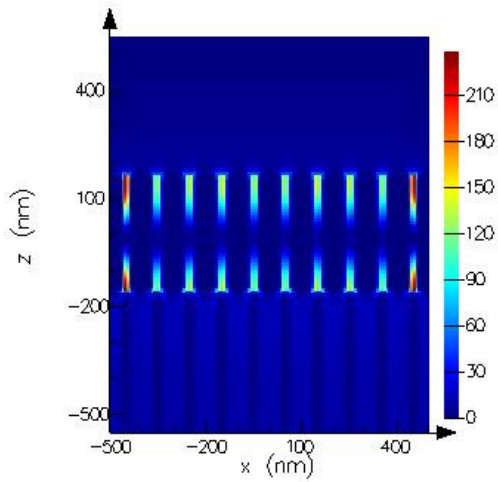


Figure 8.  $xz$ -plane intensity enhancement at 1440 nm for  $x$ -pol. source.

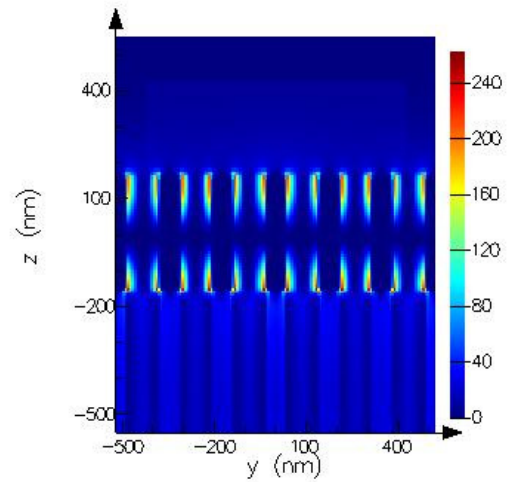


Figure 10.  $yz$ -plane intensity enhancement at 1410 nm for  $y$ -pol. source.

central part of the array farthest from the boundaries, where the effect of boundary truncation is the less. The field maxima are aligned with the source polarization, aligned between the rods. The recorded field maximum is very close to the boundary, which leads to consider a better prediction of the final performance the values around 130 that can be found near the center. Fig. 8 shows the enhancement in the  $xz$ -plane, which shows clearly how the hot-spots are placed at the interface for maximum interaction with the substance. Similar hot-spots are found at the bottom of the rods, while minor enhancement is found inside the air channels below the rods.

In the case of  $y$ -polarization, we show in Fig.9 the interface which, due to the rods displacement in the  $x$ -direction, bears hot-spots displaced along the diagonals between the rods. However, examining the central region where the field is flatter, we find good evidence of higher enhancement around

350 due to the tighter coupling between the rods in this direction. The maxima are also more numerous and more broadly distributed, which increases interaction with the sample, as can be seen by examining the  $yz$ -plane cut in Fig. 10, where it is also clear that the field is strictly confined around the rods.

## REFERENCES

- [1] H. Masuda and K. Fukuda, "Ordered Metal Nanohole Arrays Made by a Two-Step Replication of Honeycomb Structures of Anodic Alumina," *Science* 268, 1466-1468 (1995)
- [2] T. Kondo, K. Nishio, and H. Masuda, "Surface-Enhanced Raman Scattering in Multilayered Au Nanoparticles in Anodic Porous Alumina Matrix," *Applied Physics Express* 2, 032001 (2009)